Closing Remarks on Faraday Discussion 107: Interactions of Acoustic Waves with Thin Films and Interfaces

Stephen J. Martin
Microsensor Research and Development Department
Sandia National Laboratories
Albuquerque, NM 87185-1425 U.S.A.

Sandia is a multiprogram laboratory operated by Sandia Corporation, a Lockheed Martin Company, for the United States Department of Energy under contract DE-AC04-94AL85000.

Introduction

The papers in this Faraday Discussion represent the state-of-the-art in using acoustic devices to measure the properties of thin films and interfaces. Sauerbrey first showed that the mass sensitivity of a quartz crystal could be used to measure the thickness of vacuum-deposited metals.[1] Since then, significant progress has been made in understanding other interaction mechanisms between acoustic devices and contacting media. Bruckenstein and Shay[2] and Kanazawa and Gordon[3] showed that quartz resonators could be operated in a fluid to measure surface mass accumulation and fluid properties. The increased understanding of interactions between acoustic devices and contacting media has allowed new information to be obtained about thin films and interfaces. These closing remarks will summerize the current state of using acoustic techniques to probe thin films and interfaces, describe the progress reported in this Faraday Discussion, and outline some remaining problems. Progress includes new measurement techniques, novel devices, new applications, and improved modeling and data analysis.

Measurement techniques

Several new measurement techniques have been demonstrated for extracting

DISCLAIMER

information from acoustic devices. With thickness-shear mode (TSM) resonators, researchers have realized that measurement of resonant frequency alone is inadequate and that device damping or dissipation must also be measured. Changes in resonant frequency are related to energy storage at the device surface, while damping is related to power dissipation. Kipling and Thompson showed that a quartz resonator could be "completely characterized," from the electrical point of view, by measurement of electrical impedance or admittance over a range of frequencies near the fundamental resonance.[4] By fitting these multiple measurements to an equivalent-circuit model, parameters relating to energy storage and power dissipation can be extracted. While the data provide only two parameters, it's redundant nature gives a more accurate determination than a single-point measurement can. In this Faraday Discussion, Calvo et al. have described a voltage-controlled oscillator-based impedance analyzer that provides rapid measurements over a range of frequencies, eliminating the need for an expensive and bulky network analyzer.[5] Stellnberger et al. have described an improved oscillator circuit that allows control of the reflection phase at which oscillation occurs.[6] They have shown that for resonators operating in solution, there is a phase angle at which the device is insensitive to fluid properties. Thus, operation at this phase allows mass measurements to be made with greatly reduced sensitivity to fluid properties. (Temperature-induced viscosity changes, for example, can easily obscure the mass associated with monolayer levels of accumulation.) Rodahl et al. have extracted resonant frequency and damping information

by analyzing the decay transient from an impulse-excited quartz resonator.[7]

Novel devices and measurement configurations

A number of new device geometries have been reported that offer advantages over the conventional TSM resonator or surface acoustic wave (SAW) devices in terms of size, sensitivity, etc. White has reported on the use of flexural plate wave (FPW) devices fabricated using bulk micromachining processes on silicon.[8] These devices are smaller than TSM resonators and offer greater mass and liquid sensitivity. Moreover, they can be integrated on silicon with on-chip electronics. Gizeli has described Love mode devices with surface layers that increase surface confinement of acoustic energy.[9] These devices have been used as biosensors.

Changes in the geometrical arrangement of the acoustic device and the contacting media can aid in the extraction of physical properties. Daikhin and Urbakh have described a scheme for placing fluid between the resonator and an adjacent solid; the resulting acoustic interferometer allows more sensitive measurements of liquid loading to be made.[10] Tatsuma et al. have described a means for localized excitation of the quartz resonator with an electrode that is scanned across the device surface.[11] Rather than using a single large electrode that gives an integrated measurement of surface mass, this technique resolves mass distribution across the resonator surface.

Novel applications of acoustic technology

Acoustic devices have been applied in a number of new applications, revealing new information about films and interfaces. Teuscher et al. have used the TSM resonator to detect phase transitions in alkane films and alkanethiolate monolayers.[12] Good agreement was reported between the phase transition temperatures measured with this technique and more conventional techniques. Gilbert et al. reported using TSM resonators to study chlorine bubble evolution on an electrode during electrolysis of brine.[13] Ricco et al. measured changes in the shear storage modulus of a diacetylene monolayer during UV-induced crosslinking.[14] Reddy et al. observed polymerization and gelling of acrylamide solutions using TSM resonators.[15] Mak and Krim have measured the interaction of adsorbed monolayers of noble gases with nearly atomically smooth gold layers on quartz resonators at 77 K.[16] These measurements seem to indicate that asynchronous motion of the adsorbates is occurring with respect to the oscillating crystal surface due to the extremely weak surface-adsorbate binding. Stellnberger et al.[6] have used quartz resonators to perform detailed studies of corrosion, while Nishiyama et al.[17] and Kelling et al.[18] have used acoustic excitation to enhance or activate catalyst activity on the surface. Acoustic devices have also been used in a number of new sensing applications, including detection of mercury vapor[19] and salmonella bacteria.[20]

Modeling: Viscoelastic film on TSM resonator

Measurements obtained from acoustic devices are being interpreted with increasingly sophisticated models that provide new information about thin films and interfaces. This quantitative approach allows assumptions about the interaction mechanisms to be tested.

There is an increasing realization that in many circumstances the Sauerbrey model is an inaccurate description of the effect of a surface film on TSM resonator response. For films that are non-rigid (e.g., polymers), the shear motion imposed at the resonator/film interface can experience a significant phase lag across the film (Fig. 1). This causes elastic energy storage and viscous power dissipation in the film, resulting in a *viscoelastic* response that is quite different from that predicted by the Sauerbrey model.[1]

[Fig. 1 about here]

Calvo et al.[5], Lucklum and Hauptmann[21], Wolff et al.[22], and Bandey et al.[23] have all adopted a similar model for TSM resonator response with a viscoelastic film. In general, resonator response depends on the mechanical impedance (ratio of surface stress to particle velocity) imposed by the load on the resonator surface. Considering the shear displacement that originates at the device/film interface to propagate across the film, be reflected at the film/air interface, and then propagate back to the device/film interface, gives the following mechanical impedance Z_s contributed by the film:[24]

$$Z_s = \sqrt{\rho G}\tanh(j\omega h\sqrt{\rho/G}) \quad (1)$$

where ρ, h and G are the film density, thickness and complex shear modulus ($G = G' + jG''$, where G' is the storage modulus and G'' the loss modulus); $j = (-1)^{1/2}$. We note from Eq. 1 that when the argument (whose real part is the phase shift ϕ across the film) of the tanh function is small, $Z_s \cong j\omega\rho h$. In this regime, response does not depend on film properties (to first order) but only on the areal mass density (ρh); the frequency shift contributed by the film follows the Sauerbrey equation.[1]

For more complicated geometries involving multiple viscoelastic layers (Fig. 2), Bandey et al. have described a methodology for calculating the surface mechanical impedance.[23] Beginning with the mechanical impedance at the interface to the outermost region, Z_{n+1}, the impedance at the interface to the nth layer immediately before it is [ ]:

$$Z_n = Z_c^{(n)}\left[\frac{Z_{n+1}\cosh(\gamma_n h_n) + Z_c^{(n)}\sinh(\gamma_n h_n)}{Z_c^{(n)}\cosh(\gamma_n h_n) + Z_{n+1}\sinh(\gamma_n h_n)}\right] \quad (2)$$

where $Z_c^{(n)} = (\rho_n G_n)^{1/2}$ is the characteristic impedance and $\gamma = j\omega(\rho_n/G_n)^{1/2}$ is the propagation factor for the nth layer. To begin the process, we note that for a semi-infinite region, $Z_{n+1} = Z_c^{(n+1)}$. Through successive iterations of this equation, one arrives at the mechanical impedance at the quartz surface ($Z_s = Z_1$).

[Fig. 2 about here]

When the mechanical impedance is known for a given load, the electrical response can be calculated using either the transmission line model[25] or the lumped-element model.[26] The transmission line model is more accurate and cumbersome, but can be reduced to the simpler lumped-element model when $Z_s \ll Z_q$, where Z_q is the quartz characteristic impedance: $Z_q = (\rho_q \mu_q)^{1/2}$, where ρ_q and μ_q are the quartz density and shear stiffness. There is some dispute about when this criterion is satisfied, but Cernosek et al. have argued[27] that the models give 1% agreement in calculated responses as long as $Z_s \lesssim 0.2\, Z_q$.

Using the lumped-element model, a single viscoelastic film produces an electrical motional impedance[24] (Z_e in Fig. 3) that can be decomposed into a motional resistance R_2 and reactance $X_2 = \omega L_2$:

$$Z_e = R_2 + jX_2 = \frac{N\pi}{4K^2\omega C_o}\left(\frac{\rho G}{\rho_q \mu_q}\right)^{\frac{1}{2}} \tanh\left(j\omega h\sqrt{\rho/G}\right) \qquad \textbf{(3)}$$

where N is the harmonic number; $\omega = 2\pi f$, where f is the excitation frequency; C_o is the static capacitance; and K^2 is the quartz electromechanical coupling coefficient. Eq. 3 is a transcendental equation that cannot be inverted to give the film moduli in terms of R_2 and X_2 except in certain limiting cases. In these Discussions, Wolff et al. have shown that the frequency shift arising from an acoustically thin viscoelastic film is approximated by:[22]

$$\frac{\Delta f}{f_o} \cong -\frac{2f_f}{Z_q} m\left[1 + J(\omega)\frac{4\pi^2 m^2}{3\rho} f^2\right] \qquad \textbf{(4)}$$

where J (= $1/G$) is the film's shear compliance, $m = \rho h$ is the areal mass density, and f_f the fundamental resonant frequency. The first term arises from mass loading (Sauerbrey expression), while the second is a viscoelastic contribution.

[Fig. 3 about here]

Several observations can be made regarding the viscoelastic model:

(1) Films must be sufficiently thick (phase shift ϕ within an order of magnitude of $\pi/2$) for film viscoelastic properties to be extracted; for $\phi \ll \pi/2$, viscoelastic properties do not affect response (to first order).

(2) The problem of extracting film properties is under-determined: the model contains four unknowns (ρ, h, G', G''), while resonator measurements provide two quantities (R_2, X_2). In order to determine the four film parameters, it is helpful to combine acoustic measurements with other techniques. For example, Bandey et al.[23] have measured the charge passed during polymer electrodeposition to estimate film thickness; Crooks et al.[28] have combined ellipsometry and SAW measurements for simultaneous thickness and mass measurement; Grate et al.[29] have combined both SAW and TSM measurements for determination of film absorption; Hillman et al. have combined neutron reflection with TSM measurements for simultaneous determination of film density and mass changes; Crossen et al. have used scanning acoustic microscopy to obtain density scans that are resolved in the thickness direction.[30]

(3) Bandey et al.[23] and Wolff et al.[22] have shown how measurements made at several

harmonics can be used to provide independent measurements from which to determine the unknown parameters. There is some question, however, as to whether the moduli can be considered constant (frequency independent) between harmonic measurements. In the glassy or rubbery regimes, moduli do not change appreciably; in the glass-to-rubber transition region, they do. Wolff et al. have assumed that elastic moduli follow a power-law frequency dependence to utilize measurements made at different harmonics.[22]

(4) The uniqueness of the solution to the viscoelastic problem has also been questioned. Lucklum and Hauptmann have observed that several minima arise in the error function when fitting film parameters.[21] Care must be taken to find the global minimum, assuring the best determination of parameter values.

(5) Several researchers, including Calvo et al.[5] and Rodahl et al.[7], have observed that parametric representation of the data can be used to eliminate some parameter(s). Plotting R_2 vs. X_2 while varying film thickness, for example, gives a characteristic curve (for each G',G'' combination) that can be fit to a data set to determine G' and G'' without knowing film thickness.

(6) Bandey et al. have described a multilayer model, consisting of a trapped fluid layer (acting as an ideal mass layer), a finite viscoelastic layer, and a semi-infinite fluid.[23] The large number of unknown parameters contained in this model were determined stepwise: the fluid properties were extracted from measurements made on the fluid alone; these properties were then fixed while fitting the responses measured periodically as an

interfacial polymer layer was electrodeposited.

Modeling: Viscoelastic film on SAW device

Film properties have also been extracted using SAW devices. A propagating surface wave translates and deforms the film overlay, probing mass and viscoelastic properties of the film. The situation is somewhat more complicated than with the TSM resonator, however. With the TSM resonator, displacement is nearly uniform across the device surface, with strains arising only across the film due to inertial lag (in acoustically thick films). In the SAW device, however, displacement reverses every half wavelength along the surface so that in-plane strains are applied to the film (regardless of acoustic thickness) in addition to cross-film strains arising from inertial lag. For acoustically thin films, displacement is nearly uniform across the film (Fig. 4) and the SAW response is related to film properties by:[31]

$$\frac{\Delta\alpha}{k_o} - j\frac{\Delta v}{v_o} = j\omega h \sum_{i=1}^{3} c_i \left(\rho - \frac{E^{(i)}}{v_o^2} \right) \qquad (5)$$

where $\Delta\alpha/k_o$ and $\Delta v/v_o$ are the changes in attenuation per wavenumber and fractional velocity shift introduced by the film; c_i and $E^{(i)}$ are the normalized particle displacements and deformation moduli associated with surface displacements in the x-, y-, and z-directions [$E^{(1)} = G$, $E^{(2)} \cong 0$, $E^{(3)} = 4G(3K + G)/(3K + 4G)$, where K and G are the film's (complex) bulk and shear moduli]; ρ and h are the film density and thickness. The

first term on the right-hand-side of Eq. 5 arises from film translation, while the second arises from film deformation. (A more complicated model must be invoked if the film is acoustically thick[26]; Ricco et al. have argued that with polymer films this is almost always true.[14])

[Fig. 4 about here]

Ricco et al. have shown that changes in SAW response measured while photo-crosslinking a diacetylene film can be used to infer the changes induced in the film viscoelastic properties: G' increased by 5×10^{10} dyne/cm^2 due to cross-linking, similar to a rubber-to-glass transition in a polymer.

The SAW device responds as a gravimetric detector to a film overlay provided: (1) the film is acoustically thin, and (2) film viscoelastic properties do not change significantly. (The latter condition does not arise with the TSM resonator since in-plane strains are insignificant.) Interpreting responses gravimetrically, Crooks showed that diisopropyl methylphosphonate (DIMP) adsorption on a Cu^{2+}-terminated mercaptoundecanoic acid (MUA) monolayer can be measured with a SAW sensor.[28] Grate et al. showed that polymer films on SAW sensors can be used to determine gas/vapor partition coefficients.[29] They noted, however, that when films were initally glassy ($G' \approx 10^{10}$ dyne/cm^2) vapor-induced plasticization caused a *viscoelastic* response comparable to that arising from the mass of the absorbed species. When the polymer film was initially rubbery, however, the plasticization-induced modulus changes produced a response much

smaller than that arising from the mass of the absorbed species and could be neglected. Extra care must be taken in interpreting SAW responses gravimetrically.

Modeling: Simple model for fluid interaction

The interaction of acoustic devices with a contacting fluid is also being described with increasing sophistication. In the simplest model for TSM resonator response to fluid loading (Fig. 5), the resonator surface is presumed to be perfectly smooth and undergo pure shear (in-plane) displacement. A non-slip boundary condition is assumed at the solid-liquid interface, i.e., particle velocity on the liquid side matches that on the solid side. The fluid is taken to be a semi-infinite Newtonian fluid, characterized by a constant (amplitude- and frequency-independent) density, ρ, and viscosity, η. The in-plane oscillations of the device surface generate plane-parallel laminar flow in the adjacent fluid:[3]

$$v_x(y) = v_{xo}\, e^{-y/\delta} \cos(y/\delta)\, e^{j\omega t} \qquad (6)$$

where v_x is the in-plane fluid velocity, v_{xo} is the surface particle velocity, and

$$\delta = \left(\frac{2\eta}{\omega\rho}\right)^{\frac{1}{2}} \quad . \qquad (7)$$

Eq. 6 represents a critically-damped shear wave radiated into the fluid by the oscillating device surface (Fig. 5); δ is the decay length ($\delta \cong 0.25\ \mu$m for water at 20°C at 5 MHZ) that characterizes the depth of the liquid layer probed by the device.

[Fig. 5 about here]

The formalism described above can be used to determine the electrical response of the TSM resonator with fluid loading. The mechanical impedance due to the semi-infinite fluid is:[26]

$$Z_s = \left(\frac{\omega\rho\eta}{2}\right)^{\frac{1}{2}}(1+j) \qquad \textbf{(8)}$$

and the corresponding equivalent-circuit elements (Fig. 3) are:[26]

$$R_2 = X_2 = \frac{N\pi}{4K^2C_o}\left(\frac{\rho\eta}{2\omega_s\rho_q\mu_q}\right)^{\frac{1}{2}}. \qquad \textbf{(9)}$$

The motional reactance X_2 leads to a change, Δf, in the series resonant frequency of the device:[26]

$$\Delta f = -\frac{f_s^{3/2}}{N}\left(\frac{\rho\eta}{\pi\rho_q\mu_q}\right)^{\frac{1}{2}} \qquad \textbf{(10)}$$

in agreement with that reported earlier by Kanazawa and Gordon.[3]

When the simple model outlined above (Eqs. 9 and 10) is compared with experimental results using simple fluids (Fig. 6), both frequency shift and damping vary linearly with $(\rho\eta)^{1/2}$, as predicted (dashed line).[26] Using a very smooth device (average roughness $<$ 10 nm, much smaller than the decay length δ = 250 nm), the magnitude of these responses is only slightly higher than predicted. With a rough device (ave.

roughness of 243 nm, comparable to δ), Δf greatly exceeds the prediction while R_2 slightly exceeds it. The reasons for these discrepancies will be described below.

[Fig. 6 about here]

Fluid loading model enhancements

The assumptions underlying the simple fluid loading model of TSM resonator response can be modified to provide more comprehensive models. Researchers have considered the effect of compressional wave generation, surface roughness, non-Newtonian fluid behavior, liquid ordering at the interface, and interfacial slip. We will consider if and when each of these enhancements to the simple model is needed.

Compressional wave generation The simple one-dimensional model outlined previously does not account for variations in shear displacement across the crystal surface that arise due to the finite lateral extent of the resonator. From continuity considerations[32], these gradients lead to compressional wave generation by the predominantly shear-mode device. Schneider and Martin[33] have shown that compressional wave radiation provides an additional loss mechanism over viscous damping (Eq. 9) that precisely accounts for the excess dissipation (increase in R_2 over Eq. 9) measured with a smooth device. Rough devices have additional dissipation mechanisms.

Surface roughness Several researchers have noted that a rough surface can "trap" a quantity of fluid in surface pits.[34,35] Since this fluid is constrained by the pit's sidewalls to move synchronously with the surface oscillation, it contributes an additional response

nearly identical to an ideal mass layer. The major effect, then, is an additional frequency shift related to the areal mass density of the trapped fluid.[34] In Fig. 6, the rough device exhibits a significant increase in frequency shift Δf (with little change in R_2) over the smooth device due to this trapping phenomenon. Plotting frequency shift vs. surface roughness[26], moreover, indicates that even the "smooth" device may have enough roughness to account for the slight increase in Δf over that predicted for an ideally smooth surface (dashed line calculated from Eq. 10). It is, in fact, difficult to obtain a device with a sufficiently smooth surface to neglect the influence of surface roughness on resonant frequency. We note that dissipation (R_2) increases slightly with surface roughness also.

In this Discussion, Daikhin and Urbakh have shown that only pits that are small compared with the liquid decay length, and having sufficiently steep side walls, trap fluid in the sense described above.[10] For large, shallow asperities, fluid motion extends inside the pit and the quantity of trapped fluid is less than the pit volume.

Assuming an ideally smooth surface, Eq. 9 shows that both the energy storage and power dissipation (and hence frequency shift and damping) due to liquid loading depend only on the density-viscosity product ($\rho\eta$) of a contacting fluid. Thus, a smooth device alone cannot be used to resolve fluid density and viscosity. Liess et al.[36], extending previous work[37], reported that fluid trapping by a periodically corrugated surface allows fluid density to be measured. They also showed that the orientation of the corrugation with respect to the surface displacement direction influences the trapping phenomenon.

Non-Newtonian fluid behavior While the Newtonian fluid description works extremely well with simple fluids having relatively low viscosity, it can be inadequate at high operating frequencies or high fluid viscosities.[38] Relaxation effects can occur when the oscillation period approaches the time required for molecular reorientation, τ, approximated by the dielectric relaxation time. In this regime, the fluid can be described by a Maxwell model[38], with

$$\eta(\omega) = \frac{\eta_o}{1 + j\omega\tau} \qquad (11)$$

where η_o is the low frequency shear viscosity. For $\omega\tau \ll 1$, $\eta = \eta_o$ and the fluid behaves as a Newtonian fluid; as $\omega\tau$ approaches 1, η becomes complex, taking on elastic characteristics. Some researchers have claimed that even water must be treated as a non-Newtonian fluid when calculating TSM resonator responses.[39] However, since $\tau \cong 80$ ps for water, $\omega\tau \cong 0.003$ at 5 MHZ, so that relaxation effects should be negligible. Moreover, the excellent agreement obtained with the simple model (Fig. 6, smooth device), shows that the added complexity of treating water as non-Newtonian is unnecessary. For oils, however, it has been shown to be necessary under certain conditions.[40]

Liquid ordering Thompson et al.[41,42] and Haardt[43] have reported fluid-loaded responses with TSM resonators that exceed that calculated from the simple model (Eqs. 9 and 10) by factors of two or more. They attribute this enhanced response to liquid *ordering* near

the interface, resulting in a layer with significantly increased viscosity (roughly 4 times bulk values[43]). A multi-layer fluid model has been proposed: (1) a layer adjacent to the surface with viscosity higher than the bulk value, (2) a transition region in which viscosity decreases to that of the bulk, and (3) a semi-infinite region having bulk viscosity. Fig. 6 shows, however, that when highly smooth surfaces (with feature sizes « δ) are used, excellent agreement is obtained with the simple model (Eqs. 9 and 10) using only a single, low frequency, bulk viscosity value. Within experimental error, there is no evidence for a response attributable to liquid ordering.

Interfacial slip The non-slip boundary condition, typically invoked at the solid-liquid interface to calculate fluid displacement, has also been questioned. When the interaction between the solid surface and a contacting medium is sufficiently weak, it is argued, there may be a *discontinuity* in particle velocity across the interface, i.e., slip. Mak and Krim have shown non-monotonic TSM resonator responses as surface coverage by a monolayer of noble gases is varied.[16] This is interpreted as arising from asynchronous motion between the oscillating resonator surface and the adsorbed monolayer due to the extremely weak interaction between the two. Similar phenomena have been reported for non-polar organic molecules adsorbed on quartz SAW devices.[44]

Thompson et al. have argued that TSM electrodes treated with a hydrophobic monolayer can also exhibit slip when operated in aqueous solutions.[45] The evidence for this assertion is an elegant series of experiments in which the liquid-loading responses

(frequency shifts) were compared between hydrophilically- and hydrophobically-treated device surfaces.[46] Fig. 7 shows the liquid-loading responses (Δf), as well as the contact angle for the hydrophobically treated surfaces, for solutions containing various concentrations of methanol in water. When the contact angle exceeds about 100°, the hydrophobic surface clearly shows a diminished response compared with the hydrophilic surface. Thompson et al. attribute this to slip (Fig. 8).

[Figs. 7 and 8 about here]

This interpretation is called into question by a series of experiments[26] in which the effect of these surface treatments was examined on devices with various surface roughnesses. Hydrophobic surface treatments diminished the liquid response with rough devices (having surface features comparable to the liquid decay length) while smooth devices were unaffected. An essential difference between smooth and rough devices is that rough devices trap fluid in addition to viscously entraining a liquid layer. It seems possible, then, that these surface treatments are modifying the fluid trapping in surface features, rather than inducing slip.

Modeling the randomly rough surface as a sinusoidally corrugated one, we calculated the penetration of fluid into the corrugations for various microscopic contact angles (Fig. 9).[26] With a hydrophilic surface (low contact angle), liquid is drawn in so that the corrugation volume is almost entirely filled with fluid. For a hydrophobic surface (high contact angle), surface tension causes liquid to be largely excluded from the

corrugation volume, i.e., air is trapped instead. For surface features on the order of 1 μm, liquid trapping diminishes drastically for contact angles between 90 - 120° (Fig. 10), precisely the range over which Thompson et al. observed a large decrease in device response (Fig. 7).[46] The significant decrease in fluid trapping over this range of contact angles (and considering the large difference in density between water and air) could account for this decrease in response. Moreover, at the highest contact angles, where liquid trapping is minimal and the liquid meniscus forms a plane that contacts the peaks, the measured response is very close to that calculated for an ideally smooth surface, as would be expected. It appears then, that surface roughness, and the peculiar way liquid penetrates microscopic surface features, is responsible for the decrease in responses arising from hydrophobic surface treatments, and not interfacial slip.

Unlike the case of viscoelastic film-loading, where increasingly sophisticated models were needed to describe TSM resonator response, the need for more sophisticated fluid loading models (non-Newtonian fluid behavior, liquid ordering, and interfacial slip) appears to have been overstated. Rather, more care is needed in using sufficiently smooth crystals in the experiments that are performed.

[Figs. 9 and 10 about here]

Unsolved problems

Uniqueness of viscoelastic properties As described above, the number of parameters required to characterize a viscoelastic film exceeds the number of parameters determined

from an acoustic measurement made in the frequency range near a single resonance. Moreover, Lucklum and Hauptmann have shown that there are a number of local minima in the fitting error which make the determination of the best solution difficult.[21] Further work needs to be done to develop techniques that insure that sufficient information is provided to obtain a unique solution to the viscoelastic problem. This may involve measurement at harmonics, combining acoustic measurements with other techniques (e.g., ellipsometry to measure thickness and/or neutron reflectivity to measure film density), and performing successive measurements to obtain properties in stepwise fashion.

Compressional wave effects Compressional waves generated by the TSM resonator are reflected by an adjacent solid surface or a liquid-air interface, leading to interference effects in the measured response. Such effects need to be eliminated or accounted for to obtain accurate measurement of film and interfacial properties in solution.

Acoustic initiation It is generally assumed that acoustic waves simply probe the properties of a thin film or interface and measure resultant reactions. White[8] and Kanazawa[47] have pointed out the significant displacement amplitudes that are excited and indicated the possibility that these may affect rates of reaction occurring at the device surface. Indeed, Nishiyama et al.[17] and Kelling et al.[18] have used acoustic excitation to accelerate catalytic activity at surfaces. The influence of acoustic amplitude on these processes needs to be considered in further detail.

Slip and liquid ordering. There was no clear consensus formed in the Discussion as to

whether slip occurs at the interface between the device surface and a contacting solution. Further work needs to be done to consider under what conditions interfacial slip can occur.

Non-homogenous films. Models have been developed for homogenous viscoelastic films on TSM resonators and composite structures consisting of viscoelastic films with a semi-infinite liquid beyond. From the Discussion, it is apparent that many electrodeposited polymers are formed with non-uniform properties. Further work needs to be done to model these structures and to devise techniques for characterizing them.

Acknowledgments

The participants are grateful to the organizers of this Faraday Discussion for assembling a first-rate collection of work and for hosting this Discussion at Leicester University. The author is also grateful to R. W. Cernosek, A. J. Ricco, and G. C. Frye at Sandia National Laboratories, as well as Prof. R. M. White at the University of California at Berkeley and Prof. A. R. Hillman of Leicester University for helpful discussions.

Figure Captions

Fig. 1. Cross-sectional view of a thickness-shear mode (TSM) resonator with a viscoelastic film coated on the upper surface. The viscoelastic film is described by four parameters: G', G'', ρ, and $h = h_t - h_q$.

Fig. 2. Model for calculating the mechanical impedance imposed on a TSM resonator by multiple viscoelastic layers.[23]

Fig. 3. Equivalent-circuit models to describe the near-resonant electrical characteristics of the TSM resonator under various loading conditions: (a) unloaded, (b) with complex impedance element Z_e to represent surface loading, and (c) with Z_e decomposed into a motional resistance R_2 and reactance $X_2 = \omega L_2$.

Fig. 4. Translation and deformation induced by a surface acoustic wave (SAW) in an acoustically thin film coated on a semi-infinite substrate.

Fig. 5. Cross-sectional view of a smooth TSM resonator contacted by a fluid. The in-plane oscillation of the surface radiates a damped shear wave into the fluid.

Fig. 6. Frequency shift (Δf) and motional resistance (R_2) vs. liquid $(\rho\eta)^{1/2}$ for several glycerol-water mixtures on TSM resonators: (a) "smooth" device with surface roughness $<$ 10 nm, (b) "rough" device with 243 nm surface roughness. The dashed line is the predicted response based on the simple model of fluid loading (Eqs. 9 and 10).

Fig. 7. Upper: measured responses of TSM resonators with hydrophilic and hydrophobic surface treatments upon immersion in methanol-water solutions[46]; Lower: variation in

density-viscosity product and contact angle (for hydrophobic surfaces) vs. methanol concentration.

Fig. 8. The diminished response caused by hydrophobic surface treatments (Fig. 7) has been attributed[46] to interfacial slip--a discontinuity in particle displacement at the solid-liquid interface--said to arise from the weak solid-liquid interaction.

Fig. 9. Calculated cross-section of the liquid meniscus formed as liquid penetrates into a sinusoidal surface feature for several values of the microscopic liquid contact angle.[26] This offers an alternative explanation to slip (Fig. 8) in explaining the diminished response observed with hydrophobic surface treatments (Fig. 7). The dashed line indicates the initial (nonequilibrium) penetration of liquid; solid lines indicate equilibrium penetration.

Fig. 10. Variation of volume penetration of liquid into a sinusoidal surface feature (Fig. 9) with liquid contact angle. Different curves are obtained for different corrugation dimensions; peak-to-peak amplitude (equal to periodicity) is indicated in nanometers next to each.[26]

References:

1. G. Sauerbrey, *Z. Phys.*, 1959, **155**, 206.

2. S. Bruckenstein and M. Shay, *Electrochim. Acta*, 1985, **30**, 1295.

3. K. K. Kanazawa and J. G. Gordon, *Anal. Chem.*, 1985, **57**, 1770.

4. A. L. Kipling and M. Thompson, *Anal. Chem.*, 1990, **62**, 1514.

5. E. J. Calvo, R. Etchenique, P. N. Bartlett, K. Singhal, and C. Santamaria, *Faraday Discuss.*, 1997, **107**, ???.

6. K-H. Stellnberger, M. Wolpers, T. Fili, C. Reinartz, T. Paul, and M. Stratmann, *Faraday Discuss.*, 1997, **107**, ???.

7. M. Rodahl, F. Höök, C. Fredriksson, C. Keller, A. Krozer, P. Brzezinski, M. Voinova, and B. Kasemo, *Faraday Discuss.*, 1997, **107**, ???.

8. R. M. White, *Faraday Discuss.*, 1997, **107**, ???.

9. E. Gizeli, M. Liley, C. R. Lowe, and H. Vogel, *Faraday Discuss.*, 1997, **107**, poster.

10. L. Daikhin and M. Urbakh, *Faraday Discuss.*, 1997, **107**, ???.

11. T. Tatsuma, S. Yamaguchi, I. Wakabayashi, K. Mori, and N. Oyama, *Faraday Discuss.*, 1997, **107**, ???.

12. J. Teuscher, L. J . Yeager, H. Yoo, J. E. Chadwick, and R. L. Garrell, *Faraday Discuss.*, 1997, **107**, ???.

13. S. L. Gilbert, A. R. Hillman, and D. R. Hodgson, *Faraday Discuss.*, 1997, **107**, poster.

14. A. J. Ricco, A. W. Staton, R. M. Crooks, and T. Kim, *Faraday Discuss.*, 1997, **107**, ???.

15. S. M. Reddy, J. P. Jones, and T. J. Lewis, *Faraday Discuss.*, 1997, **107**, ???.

16. C. Mak and J. Krim, *Faraday Discuss.*, 1997, **107**, ???.

17. H. Nishiyama, N. Saito, M. Shima, Y. Watanabe, and Y. Inoue, *Faraday Discuss.*, 1997, **107**, ???.

18. S. Kelling, T. Mitrelias, Y. Matsumoto, V. P. Ostanin, and D. A. King, *Faraday Discuss.*, 1997, **107**, ???.

19. J. J. Caron, R. B. Haskell, P. Benoit, and J. F. Vetelino, *Faraday Discuss.*, 1997, **107**, poster.

20. Y. S. Fung, S. H. Si, and S. Z. Yao, *Faraday Discuss.*, 1997, **107**, poster.

21. R. Lucklum and P. Hauptmann, *Faraday Discuss.*, 1997, **107**, ???.

22. O. Wolff, E. Seydel, and D. Johannsmann, *Faraday Discuss.*, 1997, **107**, ???.

23. H. L. Bandey, A. R. Hillman, M. J. Brown, and S. J. Martin, *Faraday Discuss.*, 1997, **107**, ???.

24. S. J. Martin and G. C. Frye, *Proc. of the 1991 IEEE Ultrasonics Symposium* (IEEE, New York) 393.

25. V. E. Granstaff and S. J. Martin, *J. Appl. Phys.*, 1994, **75**, 1319.

26. S. J. Martin, G. C. Frye, A. J. Ricco, and S. D. Senturia, *Anal. Chem.*, 1993, **65**, 2910.

27. R. W. Cernosek, S. J. Martin, A. R. Hillman, and H. L. Bandey, *Frequency Control Symp.*, Orlando, FL, May 28 - 30, 1997.

28. R. M. Crooks, H. C. Yang, L. J. McEllistrem, R. C. Thomas, and A. J. Ricco, *Faraday Discuss.*, 1997, **107**, ???.

29. J. W. Grate, S. N. Kaganove, and V. R. Bhethanabotla, *Faraday Discuss.*, 1997, **107**, ???.

30. J. D. Crossen, J. M. Sykes, T. Zhai, and G. A. D. Briggs, *Faraday Discuss.*, 1997, **107**, ???.

31. S. J. Martin, G. C. Frye, and S. D. Senturia, *Anal. Chem.*, 1994, **66**, 2201.

32. B. A. Martin and H. E. Hager, *J. Appl. Phys.*, 1989, **65**, 2627.

33. T. W. Schneider and S. J. Martin, *Anal. Chem.*, 1995, **67**, 3324.

34. R. Schumacher, J. G. Gordon, O. Melroy, *J. Electroanal. Chem.*, 1987, **216**, 127.

35. R. Beck, U. Pitterman, K. G. Weil, *J. Electrochem. Soc.*, 1992, **139**, 453.

36. H-D. Liess, A. Knezevic, M. Rother, and J. Muenz, *Faraday Discuss.*, 1997, **107**, ???.

37. S. J. Martin, G. C. Frye, and K. O. Wessendorf, *Sensors and Actuators A*, 1994, **44**, 209.

38. F. M. White, *Viscous Fluid Flow* (McGraw-Hill, New York, 1979).

39. G. Hayward et al., *Frequency Control Symp.*, Orlando, FL, May 28 - 30, 1997.

40. S. J. Martin, R. W. Cernosek, and J. J. Spates, *Digest of Technical Papers*, 8th Inter. Conf. on Solid-State Sensors and Actuators, June 25 - 29, 1995, Stockholm, Sweden, p. 712.

41. M. Thompson, C. L. Arthur, and G. K. Dhaliwal, *Anal. Chem.*, 1986, **58**, 1206.

42. L. V. Rajakovic, B. A. Cavic-Vlasak, V. Ghaemmaghami, M. R. K. Kallury, A. L. Kipling, and M. Thompson, *Anal. Chem.*, 1991, **63**, 615.

43. H. Haardt, Ph.D. Dissertation, Universität Kiel, Kiel, Germany, 1971.

44. S. J. Martin, A. J. Ricco, D. S. Ginley and T. E. Zipperian, *IEEE Transactions on UFFC*, 1971, **UFFC-34**, 142.

45. M. Thompson, A. Kipling, W. C. Duncan-Hewitt, L. V. Rajakovic, and B. A. Cavic-Vlasak, *Analyst*, 1991, **116**, 881.

46. M. Yang, M. Thompson and W. C. Duncan-Hewitt, *Langmuir*, 1993, **9**, 802.

47. K. K. Kanazawa, *Faraday Discuss.*, 1997, **107**, ???.

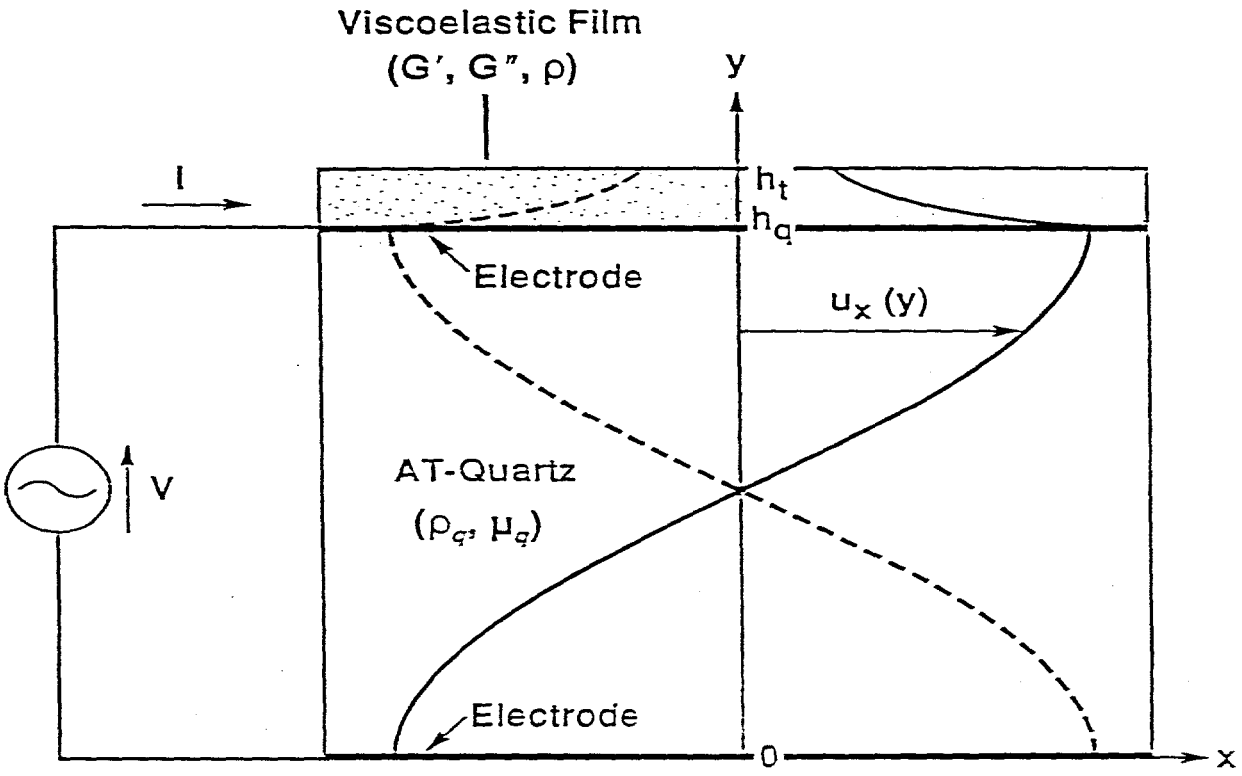
Viscoelastic Film
(G′, G″, ρ)
y
I
h_t
h_q
Electrode
u_x (y)
V
AT-Quartz
(ρ_q, μ_q)
Electrode
0
x

Fig. 1

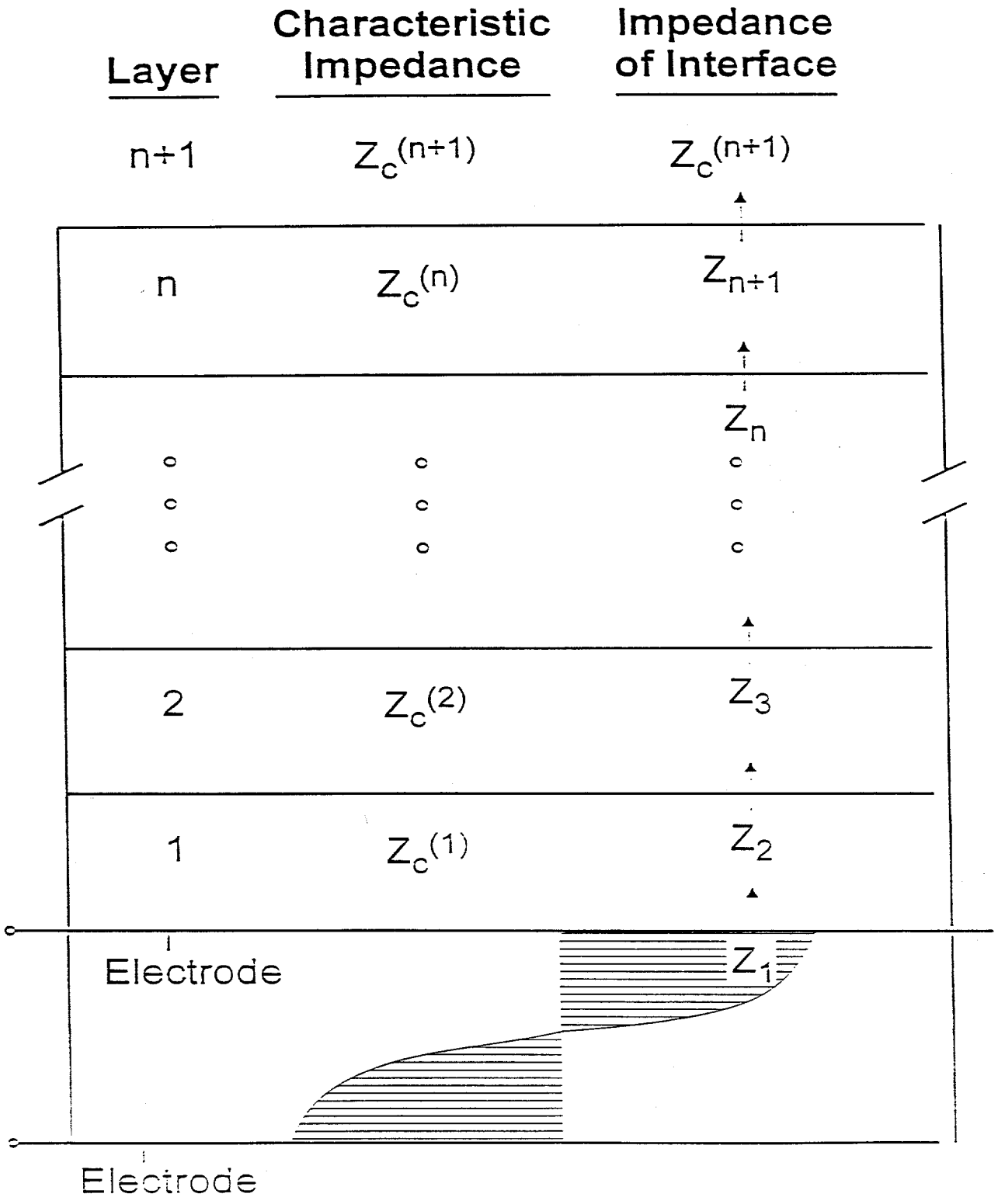
Layer
Characteristic Impedance
Impedance of Interface
n+1
$Z_c^{(n+1)}$
$Z_c^{(n+1)}$
n
$Z_c^{(n)}$
Z_{n+1}
Z_n
2
$Z_c^{(2)}$
Z_3
1
$Z_c^{(1)}$
Z_2
Z_1
Electrode
Electrode

Fig. 2

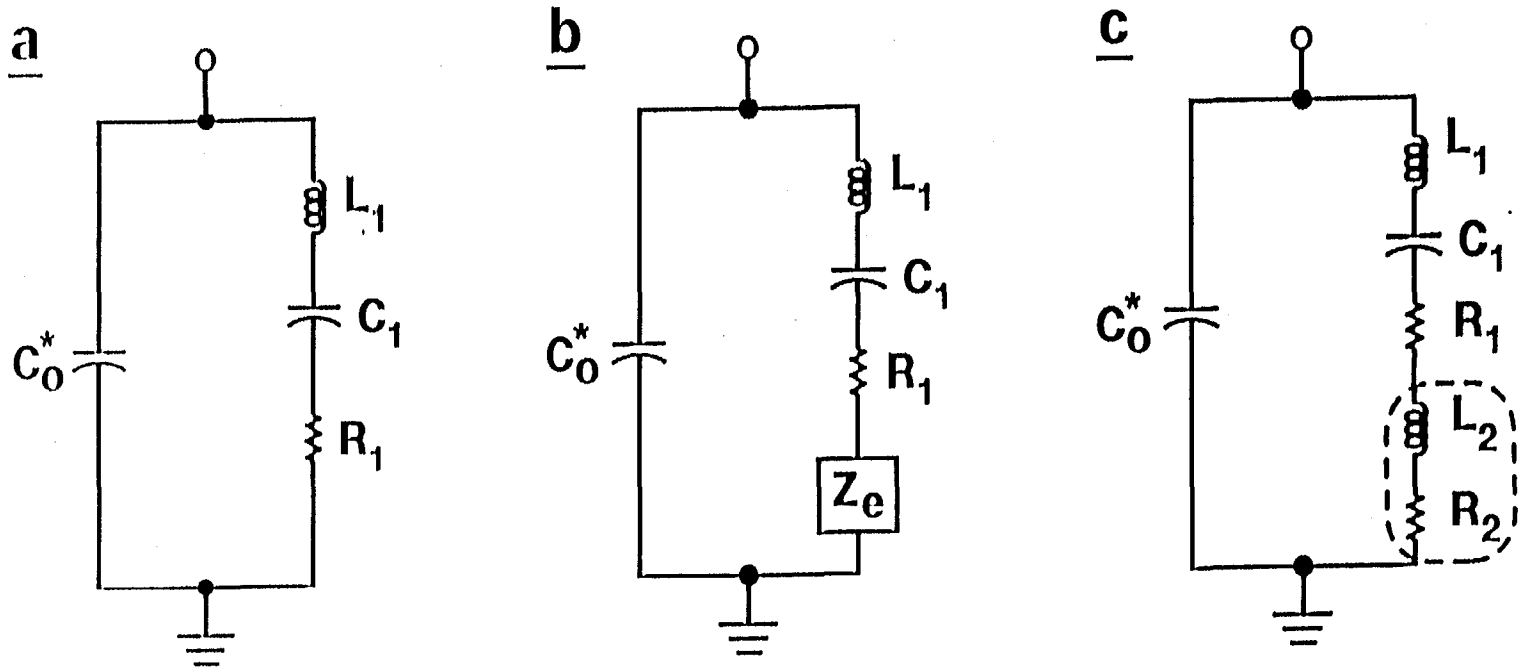

Fig. 3

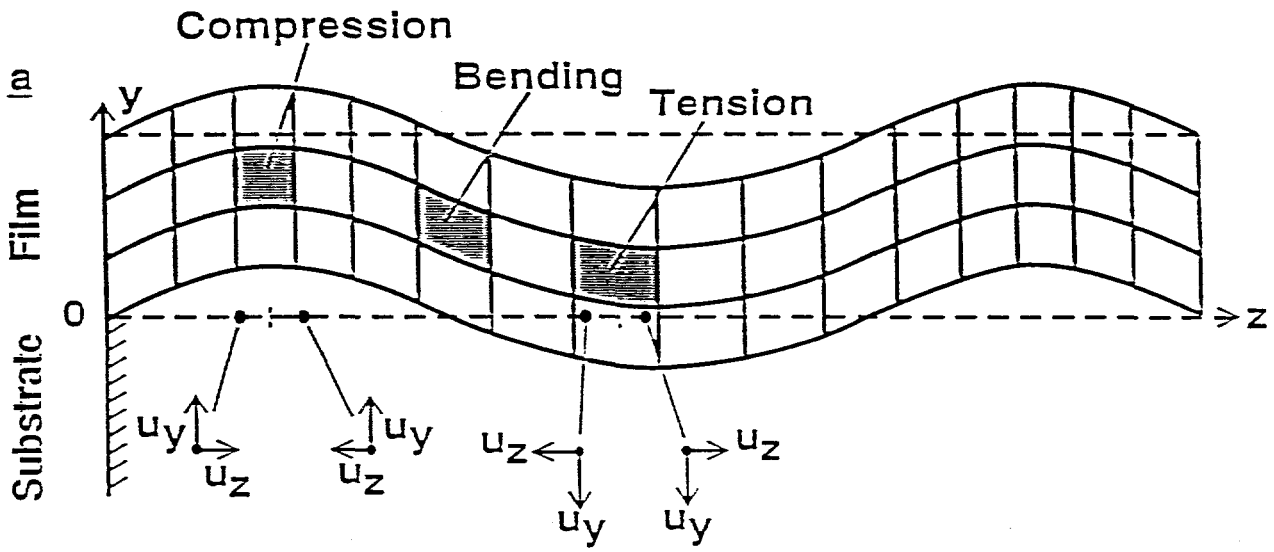
a
Compression
Bending
Tension
y
Film
Substrate
0
z
u_y
u_z
u_y
u_z
u_z
u_y
u_z
u_y

Fig. 4

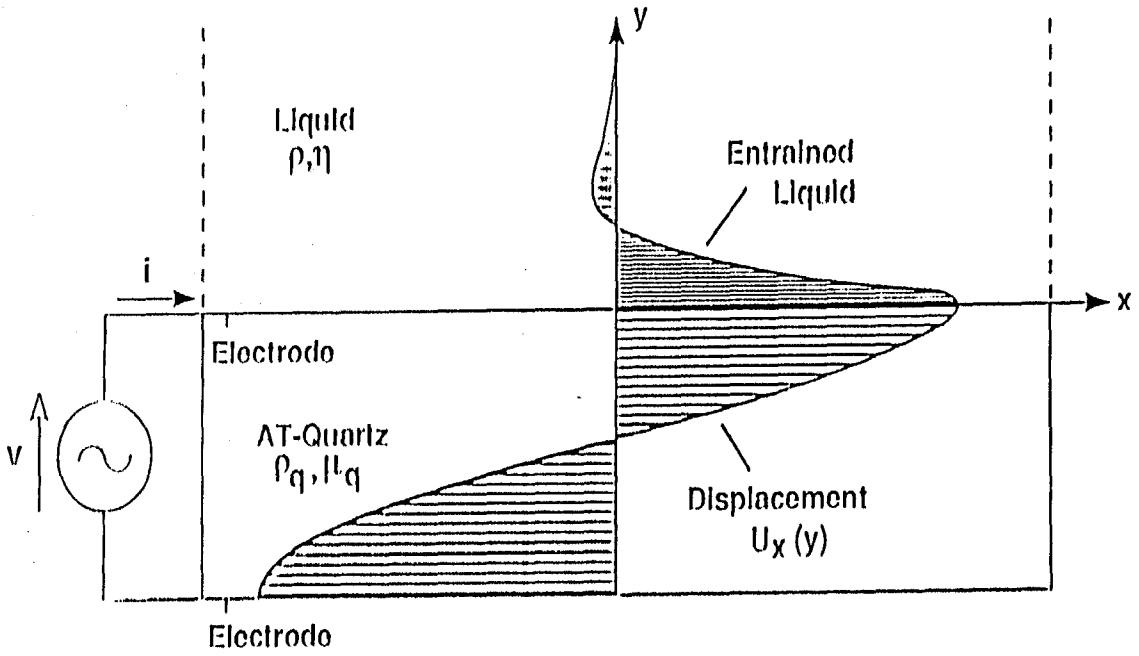
y
Liquid
ρ,η
Entrained
Liquid
i
x
Electrode
v
AT-Quartz
ρq, μq
Displacement
Ux (y)
Electrode

Fig. 5

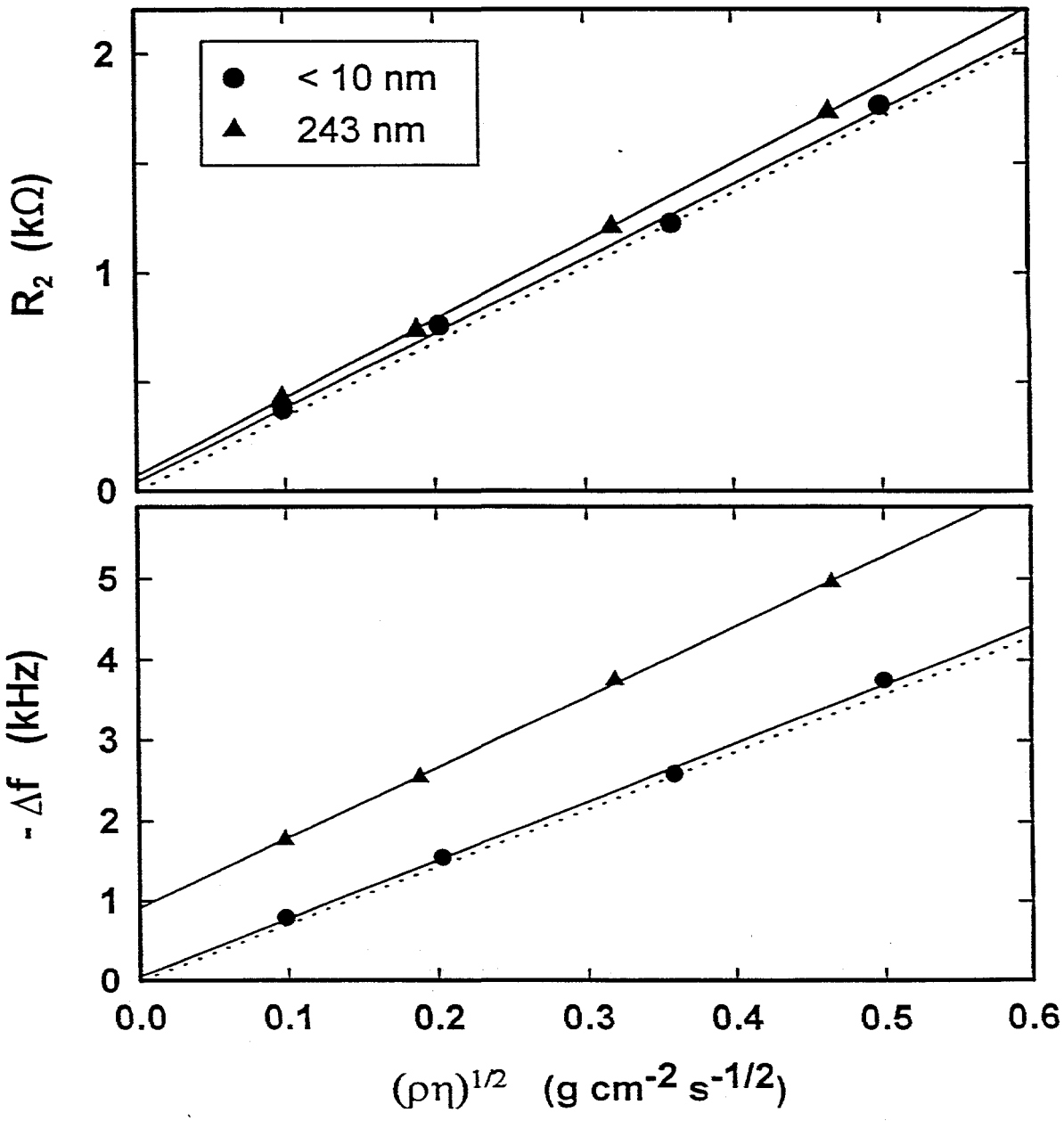

Fig. 6

file:DROPLSPS

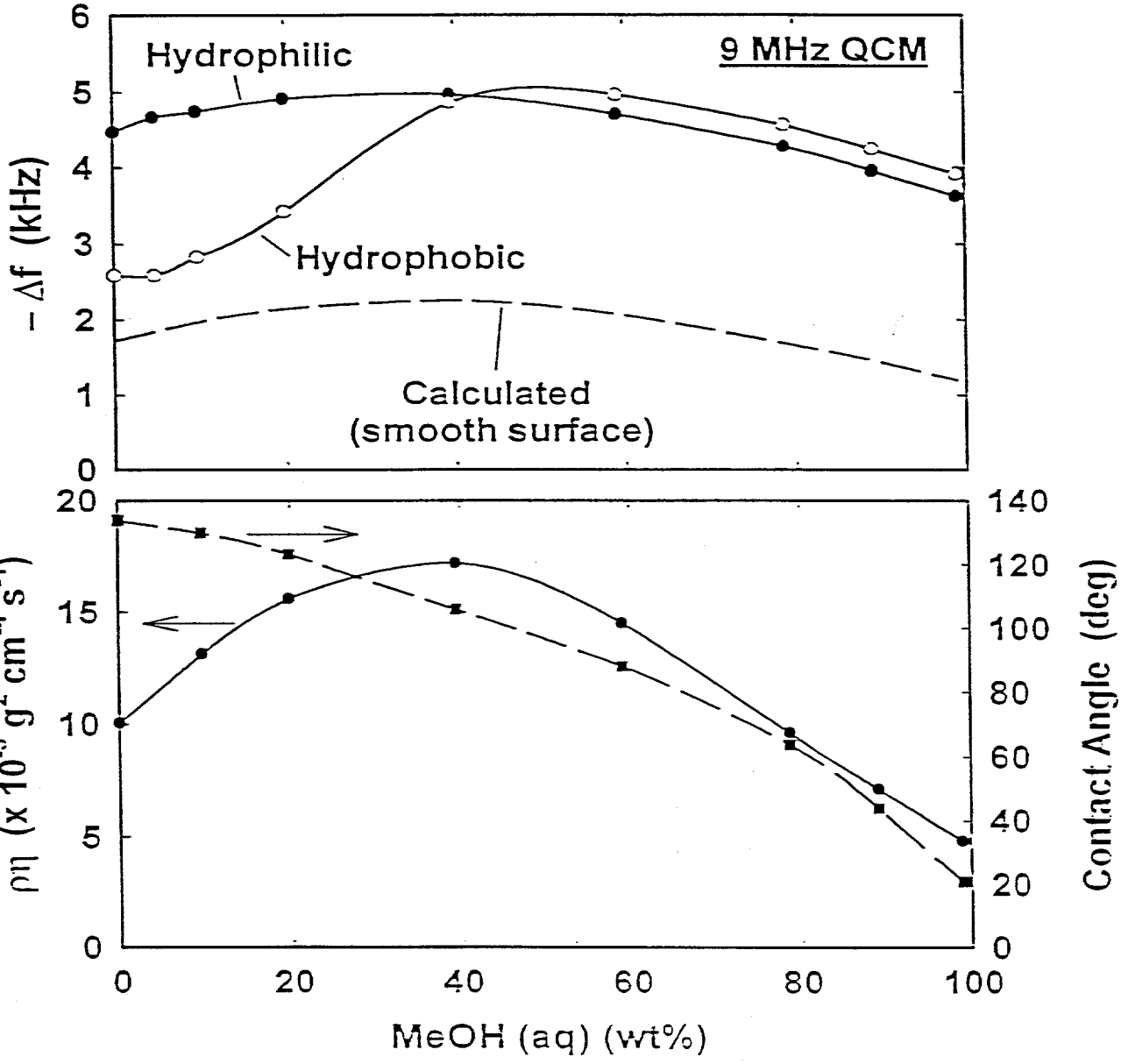
Hydrophilic
9 MHz QCM
Hydrophobic
Calculated
(smooth surface)
$-\Delta f$ (kHz)
$\rho\eta$ (x 10^{-3} g^2 cm^{-4} s^{-1})
Contact Angle (deg)
MeOH (aq) (wt%)
0
1
2
3
4
5
6
0
5
10
15
20
0
20
40
60
80
100
120
140
0
20
40
60
80
100

Fig. 7

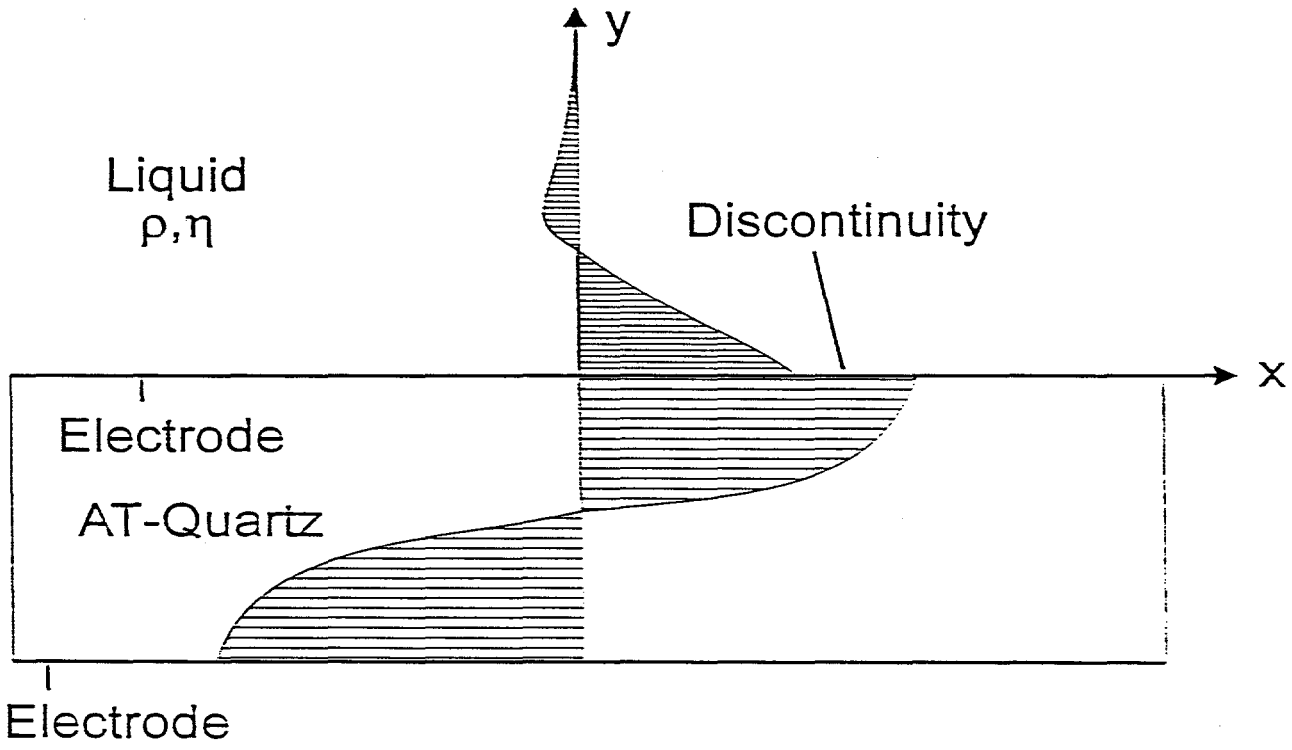

Fig. 8

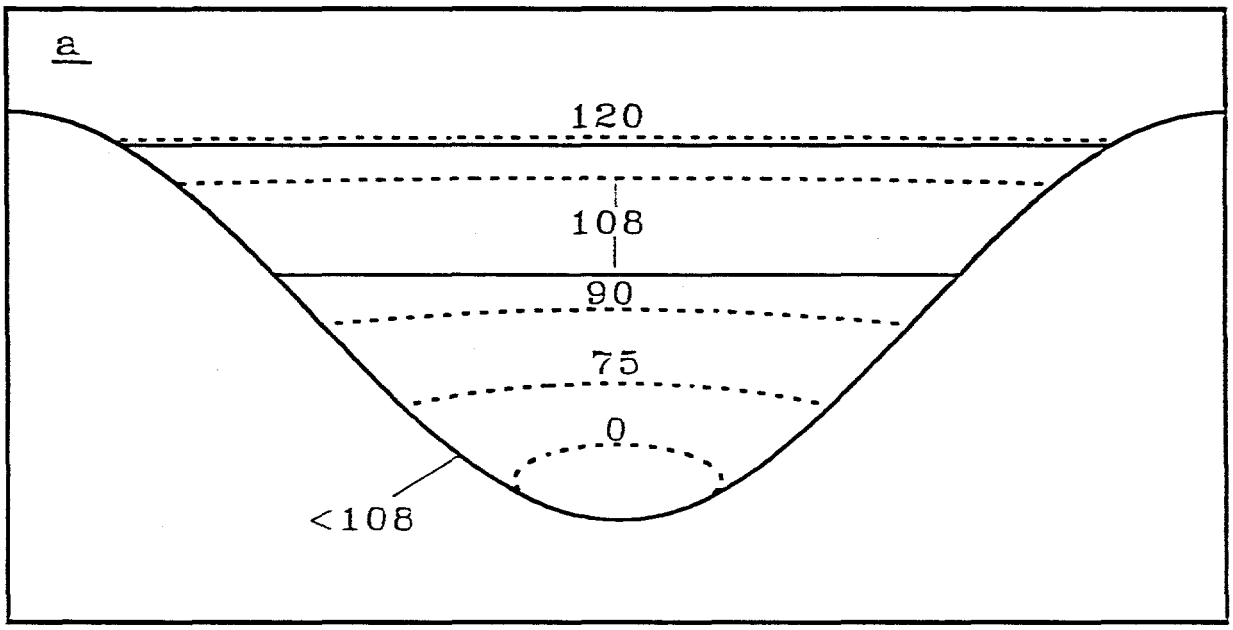

Fig. 9

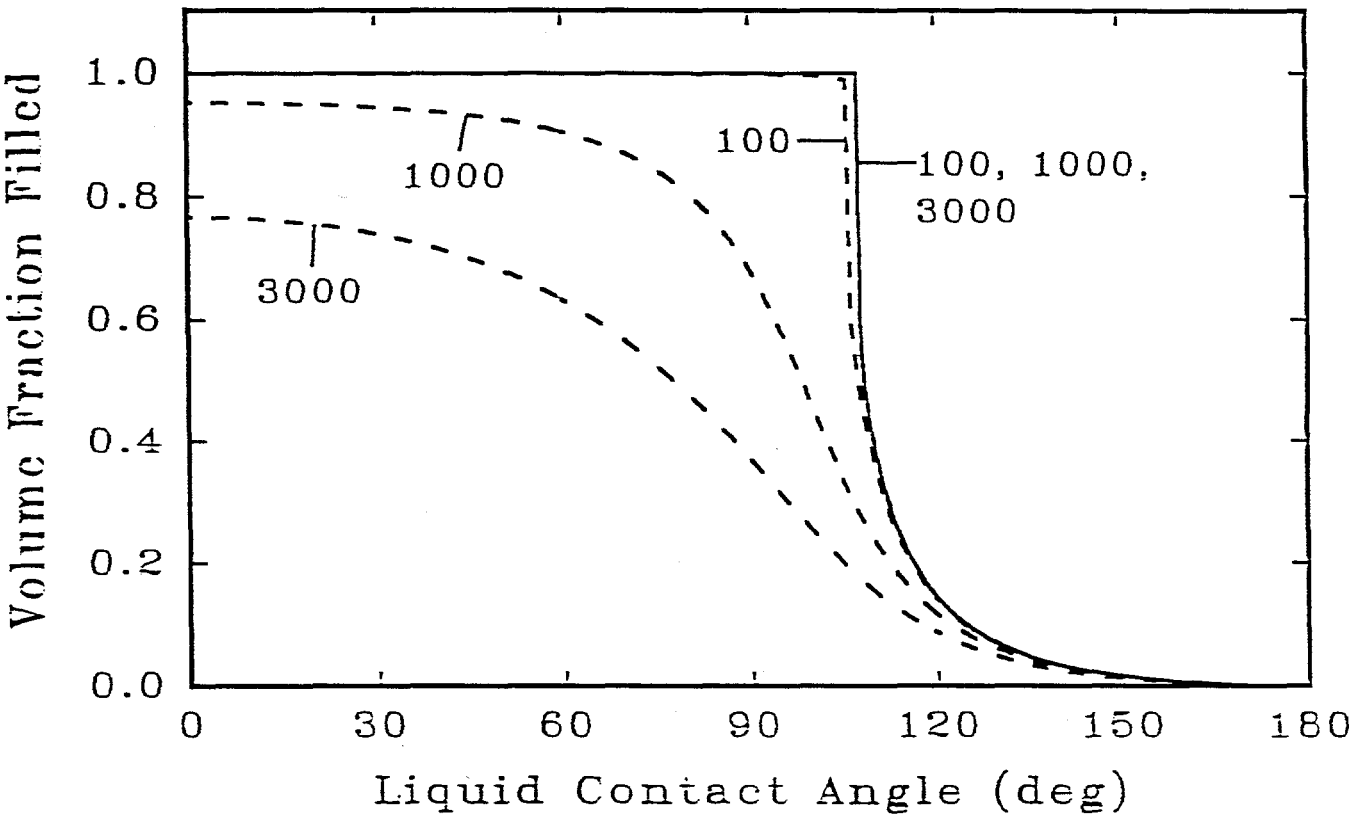
Volume Fraction Filled
1.0
0.8
0.6
0.4
0.2
0.0
0
30
60
90
120
150
180
Liquid Contact Angle (deg)
1000
3000
100
100, 1000,
3000

Fig. 10